Desalination and Water Treatment
www.deswater.com
doi: 10.5004/dwt.2019.23504

144 (2019) 9–25
March

Antifouling behavior on the linear suspension PEG-based surface and two-end-linked PEG-based surface of composite nanofiltration membranes via two-step interfacial polymerization

Xiaoli Ding[a,b], Te Kang[c], Hongyong Zhao[a,b,*], Qi Wang[a,b], Yuzhong Zhang[a,b,**], Guodong Kang[d]

[a]*State Key Laboratory of Separation Membranes and Membrane Processes/National Center for International Joint Research on Separation Membranes, Tianjin Polytechnic University, Tianjin 300387, China, emails: zhaohongyong@tjpu.edu.cn (H. Zhao), zhangyz2004cn@vip.163.com (Y. Zhang)*
[b]*Tianjin Key Laboratory of Hollow Fiber Membrane Materials and Processes, Tianjin Polytechnic University, Tianjin 300387, China*
[c]*Beijing Origin Water Technology Co., Ltd, Beijing 102206, China*
[d]*Dalian Institute of Chemical Physics, Chinese Academy of Sciences, Dalian 116023, China*

Received 13 May 2018; Accepted 21 November 2018

ABSTRACT

Hydrophilic nanofiltration membranes with single-layered or double-layered poly(ethylene glycol) (PEG) based structure were fabricated by two-step interfacial polymerization (IP) to enhance antifouling property. *O*,*O*′-bis(2-aminopropyl) polypropylene glycol-block-polyethylene glycol-block-polypropylene glycol (jeffamine) was used as monomer and modifier in both layers. The antifouling performance against bovine serum albumin (BSA) for the nascent polyamide membrane with single PEG-based layer was not satisfactory with a highest water flux recovery ratio (FRR) of 75.9%. Therefore, a second IP was performed between jeffamine and the residual unreacted chloroformyl group in selective layer to form an additional PEG-based layer, which demonstrated the two-end-linked structure when jeffamine 2003 was used and the linear suspension structure when jeffamine 600 was used. The results showed that the flux and rejection of membranes with double-layered PEG-based structure had little variation compared with that of single-layered membranes, while the antifouling performance against BSA was significantly improved by the additional PEG-based layer. Moreover, the additional linear suspension PEG-based layer contributed more to antifouling performance than the additional two-end-linked PEG-based structure. The membrane with the additional linear suspension PEG-based layer displayed a highest water FRR of 99.6%, while the membrane with the additional two-end-linked PEG-based layer displayed a highest water FRR of 83.6%.

Keywords: Antifouling; Poly(ethylene glycol) based; Linear suspension; Two-end-linked; Two-step interfacial polymerization

1. Introduction

Water treatment by membrane technology has been widely used in various applications. Nanofiltration (NF) has been a hot spot over the last decade because of excellent permeation-separation performance such as high water flux, high rejection to multivalent salts and organic molecules (molecular weights above 150), and relatively lower operating pressure compared with reverse osmosis (RO) [1]. However, in NF process, membrane fouling caused by various foulants often results in a sharp decline in flux and an increase in maintenance and operation cost. A substantial effort has been devoted to improve the antifouling property of NF membranes. Increasing hydrophilicity is widely

* Corresponding authors.

accepted because many foulants such as proteins are hydrophobic in nature [2]. Polyethylene glycol and its derivatives with C–C–O segment (poly(ethylene glycol) (PEG)-based structure) as effective hydrophilic modifiers and protein-resistant agents are widely used in the surface modification for enhancing antifouling property due to their extraordinary antifouling abilities [2–4]. PEG-based antifouling layer on selective layer can be obtained by dip coating [5], electrospray [6], layer-by-layer assembly [7], grafting [8,9], etc., which incorporate an additional layer on the selective layer, resulting in a decrease in flux, since the additional layer increases the mass transfer resistance. Therefore, the membrane with a PEG-based selective layer rather than the membrane with an additional PEG-based antifouling layer on the selective layer has been fabricated to avoid the decrease in flux in recent years. Akthakul et al. [10] coated poly (vinylidene fluoride)-g-poly(oxyethylene methacrylate) copolymer on poly(vinylidene fluoride) substrate. The resulting membrane showed no detectable fouling over the course of the 90- min filtration using oleic acid and triethanolamine as the foulant. Gol et al. [11–13] introduced C–C–O segment into polyamide (PA) selective layer of composite membranes by in situ PEGylation of monomers or mixing alkyl-amine-terminated PEG in interfacial polymerization (IP). The resulting membranes showed improved antifouling performance against bovine serum albumin (BSA, 250 mg L^{-1}) with a lowest water decline of 7.5% after 20 h. Zhao et al. [14] prepared polypiperazine-amide NF composite membrane through trimesoyl chloride (TMC) reacting with piperazine (PIP) and *O,O′*-bis(2-aminopropyl) polypropylene glycol-block-polyethylene glycol-block-polypropylene glycol (jeffamine). The resulting membrane showed improved antifouling performance in electrodialysis concentrate treatment with almost complete water flux recovery after hydraulic cleaning. Cheng et al. [15,16] fabricated PEG-based selective layer by IP of linear amino-functional PEG and TMC on polyethersulfone substrate, containing the hydrophilic two-end-linked C–C–O segment in the main chain of selective layer molecules. The resulting membrane demonstrated a high pure water flux of 66 L m^{-2} h^{-1} at 0.5 MPa with $MgSO_4$ rejection of 80.2% [15]. This membrane also displayed excellent antifouling performance against BSA with a water decline of 68% and a water flux recovery of 90.2% [16], but it could not match the membrane with C–C–O segment in the side chain of the selective layer acting as a grafted brush layer (comb-like structure/linear suspension structure) at the membrane. For example, composite NF membrane coated with the amphiphilic graft copolymer poly(vinylidene fluoride)-graft-poly(oxyethylene) methacrylate displayed a slow water decline in 1,000 mg L^{-1} BSA solution (13% after 10 d) [17]. These results may indicate that the C–C–O segment in side chain makes more significant contribution to the improvement of the antifouling performance against BSA than the C–C–O segment in main chain.

In this study, in order to investigate the contribution of the two different structures (C–C–O segment in side chain: linearity suspension structure or C–C–O segment in main chain: two-end-linked structure) to the improvement of antifouling performance, we fabricated composite PA NF membranes with single-layered PEG-based structure by one-step IP and membranes with double-layered PEG-based structure by two-step IP for systematic comparison. The first PEG-based layer was synthesized by IP between TMC and jeffamine on porous polysulfone (PSf) substrate, which acted as the selective layer with modest antifouling property. The second PEG-based layer was synthesized by another IP between the residual unreacted chloroformyl group in the first selective layer and jeffamine. Three different jeffamine monomers with different chain length were used to form the different structure in the second PEG-based layer. The surface chemistry, morphology, and physical characters, such as hydrophilicity and electronegativity, were characterized. The permeation-separation performance and antifouling performance of composite membranes were also reported. The difference between the contributions of two different structures to the improvement of the antifouling performance was investigated and discussed.

2. Experimental

2.1. Materials

PSf (P-3500) was purchased from Solvay Co., Ltd. (Shanghai, China). Jeffamine (ED600, ED900, ED2003 with an average molecular weight of 600, 900, and 2,003, respectively) were purchased from Aldrich Chemical Co. (Shanghai, China). Magnesium sulfate ($MgSO_4$, AR) were purchased from Guangfu Fine Chemical Research Institute (Tianjin, China). Disodium hydrogen phosphate (Na_2HPO_4, AR) and sodium dihydrogen phosphate (NaH_2PO_4, AR) were purchased from Kermel Chemical Reagent Co., Ltd. (Tianjin, China). TMC (98%) was purchased from Aladdin Reagent Co. (Shanghai, China). The chemical structures of monomers are shown in Fig. 1. The solvents *N*,*N*-dimethylformamide (DMF, 99.5%), ethanol (99%), *n*-hexane (98%), and 1-methyl-2-pyrrolidinone (NMP, 99%) were purchased from Fengchuan Chemical Reagent Technology Co., Ltd. (Tianjin, China). BSA (95%) as foulant was purchased from Solarbio Science and Technology Co., Ltd. (Beijing, China). Rhodamine B (M_n = 479.68 g mol^{-1}), Bromophenol blue (M_n = 670 g mol^{-1}), and Congo red (M_n = 697 g mol^{-1}) were purchased from Tianjin Guangfu Fine Chemical Research Institute (Shanghai, China). All the chemicals were used as received.

2.2. Membrane fabrication

PSf substrate was fabricated by nonsolvent-induced phase separation. PSf was dissolved in the mixture of NMP and DMF. After degassed, the casting solution was cast on nonwoven fabrics with a uniform thickness of 250 μm and then immersed into water. The as-fabricated membrane was subsequently washed in the running water for 24 h to remove the residual solvent and then kept in water prior to usage. The substrate membrane displayed a pure water flux of 328.7 L m^{-2} h^{-1} at 0.1 MPa with a molecular weight cutoff (MWCO) of 40 kDa.

The selective PEG-based layer of the composite membrane was synthesized on the PSf substrate membrane by IP. Jeffamine (ED600) was used in the aqueous solution. The aqueous solution (1 wt.%) was poured onto the top surface of substrate membranes for 5 min, and the excess

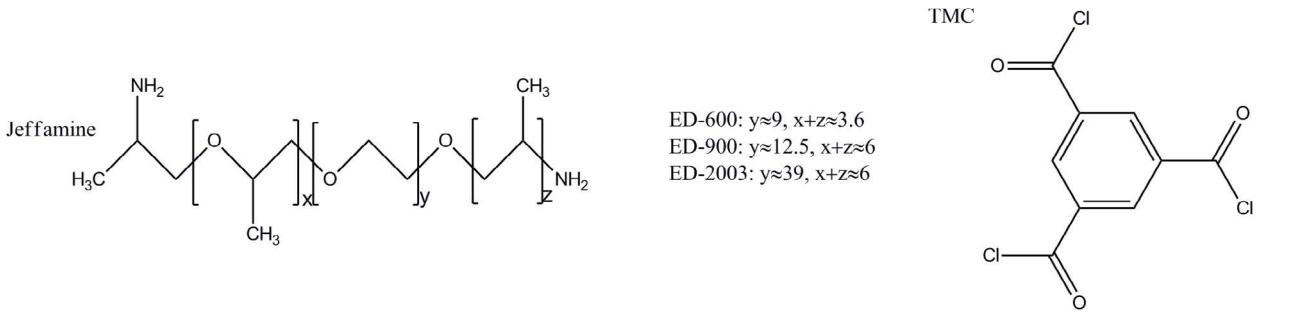

Fig. 1. Chemical structures of monomers.

solution on the surface was carefully removed by a rubber roller. Subsequently, 0.15% (m v^{-1}) TMC/*n*-hexane solution was poured onto the substrate membrane soaked by aqueous solution to form the selective layer. After being washed in *n*-hexane to remove the unreacted TMC, some nascent composite membrane was heated in vacuum oven at 60°C for 3 min to obtain the composite membrane with single PEG-based layer, identified as XX-Com-S, where XX was the aqueous monomer used in the first IP to form the selective layer. Some nascent composite membranes with single-layered PEG-based structure were modified by a second IP to form the composite membrane with double-layered PEG-based structure, where the residual unreacted chloroformyl group from the first cross-linked layer reacted with amino group in jeffamine. This method had been used in modification of RO membranes [18] and forward osmosis (FO) membranes [19], details were not displayed here for brevity. After being washed in deionized water, ethanol, and *n*-hexane successively, the composite membrane was also heated in vacuum oven at 60°C for 3 min to obtain the composite membrane with double-layered PEG-based structure, identified as YY-XX-Com-D, where YY was the aqueous monomer used in the second IP. The whole process is presented in Fig. 2.

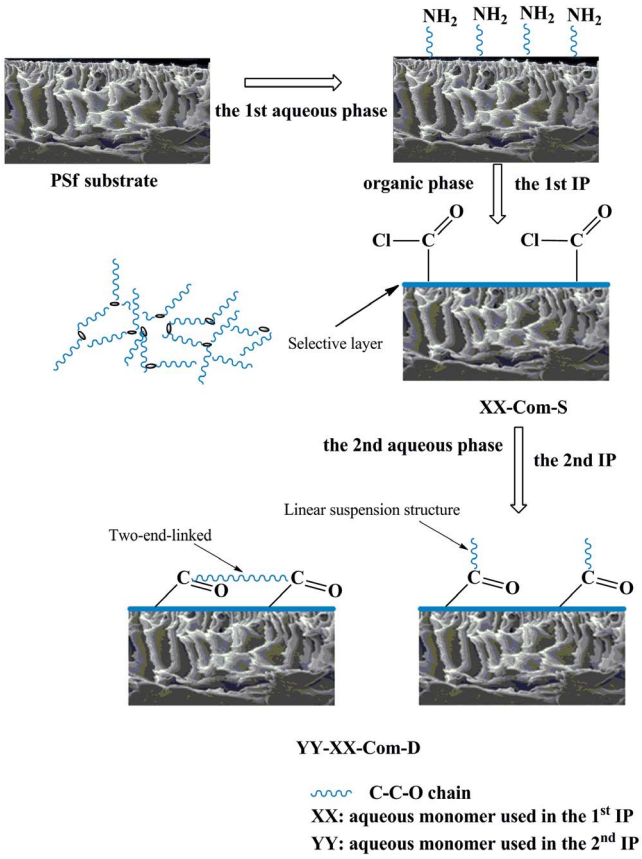

Fig. 2. The two-step IP process used to fabricate composite membranes with single-layered or double-layered PEG-based structure.

2.3. Membrane characterization

Attenuated total reflection Fourier transform infrared spectroscopy (FTIR, Bruker Vector-22, Germany) was used to confirm the reaction between TMC and jeffamine. For each measurement, the membrane sample was scanned at 4 cm^{-1} resolution from 400 to 4,000 cm^{-1} range. X-ray photoelectron spectroscopy (XPS, Thermofisher, USA) was used to characterize the surface elemental content of membranes using an Al K alpha X-ray source, which was also used to confirm the reaction between TMC and jeffamine. Field emission scanning electron microscope (FESEM, Hitachi S-4800, Japan) was used to study the surface and cross-sectional morphologies. Atomic force microscopy (AFM, Nanoscope 3, Agilent, USA) was used to determine the surface roughness quantified as the root-mean-square roughness (R_{ms}) in tapping mode at a scanning rate of 1.2 Hz. Zeta-potential analysis meter (Anton Paar, SurPASS, Austria) was used to determine the surface charge property of composite membranes quantified as zeta-potential (mv). The measurements were conducted at pH 7 and 25°C. Contact-angle meter (SL200KB, USA) was used to measure the contact angle (◦) of the pure water on the membrane surface, characterizing the hydrophilicity of the membrane surface.

2.4. Flux and rejection measurement

The flux and rejection measurements were performed in a stainless permeation cell at room temperature and 0.5 MPa. Before test, membranes were placed in the permeation cell and operated under 0.5 MPa for 0.5 h to make sure the stability of the test. The flux (J, L m^{-2} h^{-1}) was calculated using the following equation:

$$J = \frac{V}{A \times t} \quad (1)$$

where V (L) is the water volume collected in the permeate side, fixed at 10 L × 10^{-3} L in this study, A (m^2) is the active membrane area, fixed at 1.96 m^2 × 10^{-3} m^2 in this study, and t (h) is the collection time.

The rejection (R) was calculated using the following equation:

$$R = \left(1 - \frac{C_p}{C_f}\right) \times 100\% \quad (2)$$

where C_p (mol L^{-1}) and C_f (mol L^{-1}) are the salt concentrations in the permeate and feed solution, respectively, determined from the conductivity measured by an electrical conductivity (DDS-11A, Shanghai Hongyi Instrument Co., Ltd., China).

2.5. MWCO determination

Aqueous solutions of dyes were filtered through membranes to determine the MWCO (Da) at 0.5 MPa. These dye solutions were prepared by dissolving dyes at a concentration of 50 mg L^{-1} in deionized water. The concentration of dyes was determined by ultraviolet spectrophotometer (Beijing Puxi, T6). The MWCO is defined as the solute molar mass at which the rejection is more than 90%.

2.6. Fouling resistance testing

BSA was dissolved in the phosphate-buffered saline solution (pH = 7.4) with the concentration of 1,000 mg L^{-1} as foulant, which was kept in an ice water bath to prevent the protein inactivation. The test was operated at room temperature and at 0.5 MPa. The fouling resistance test was conducted in three steps: (1) pure water flux test for 1 h, (2) fouling process: water flux test with BSA solution for 8 h, and (3) water backwashing process for 1.5 h. Normalized flux (J_N) was used to evaluate the flux change of composite membranes, calculated by the following equation:

$$J_N = \frac{J_t}{J_0} \quad (3)$$

where J_0 (L m^{-2} h^{-1}) is the initial water flux, calculated after the first 10-mL collection, and J_t (L m^{-2} h^{-1}) is the real-time water flux. The total water flux decline ratio (DRt, %) and water flux recovery ratio (FRR, %) were used to evaluate the antifouling performance of composite membranes. The DRt caused by BSA fouling was defined and calculated using the following equation:

$$\mathrm{DRt} = \frac{J_{w1} - J_p}{J_{w1}} \times 100\% \quad (4)$$

where J_{w1} (L m^{-2} h^{-1}) is the water flux tested at the end of step (1) before BSA solution feeding and J_p (L m^{-2} h^{-1}) is the water flux tested after BSA solution feeding for 8 h.

Water FRR was defined and calculated using the following equation:

$$\mathrm{FRR} = \frac{J_{w2}}{J_{w1}} \times 100\% \quad (5)$$

where J_{w2} (L m^{-2} h^{-1}) is the water flux tested after water backwashing for 1.5 h.

The ratio of reversible fouling over the total fouling (R_r, %) and the ratio of irreversible fouling over the total fouling (R_{ir}, %) were defined and calculated using the following equations, respectively:

$$R_r = \left(\frac{J_{w2} - J_p}{J_{w1} - J_p}\right) \times 100\% \quad (6)$$

$$R_{\mathrm{ir}} = \left(\frac{J_{w1} - J_{w2}}{J_{w1} - J_p}\right) \times 100\% \quad (7)$$

3. Results and discussion

3.1. Surface chemistry

The FTIR spectra of ED600-Com-S, ED600-ED600-Com-D, ED900-ED600-Com-D, and ED2003-ED600-Com-D are shown in Fig. 3. The characteristic peak of ED600 amide at 1,660 cm^{-1} (C=O stretching vibration) could be found on ED600-Com-S and ED600-ED600-Com-D. The spectra showed broad characteristic peaks in the range of 2,880–3,000 cm^{-1} (–CH_2–) because of C–C–O repeat units in jeffamine [20]. There was no obvious difference between the spectrum of ED600-Com-S and membranes with double PEG layers, which indicated that no definite evidence existed in FTIR spectra to support the second IP.

XPS analysis was conducted to further determine the surface elemental compositions of composite membranes and then support the second IP. As shown in Fig. 4, the intense signs of XPS peaks for oxygen, carbon, and nitrogen elements appeared in the spectra of PSf substrate, ED600-Com-S, ED600-ED600-Com-D, ED900-ED600-Com-D, and ED2003-ED600-Com-D. Compared with PSf substrate, the composite membrane contained a higher proportion

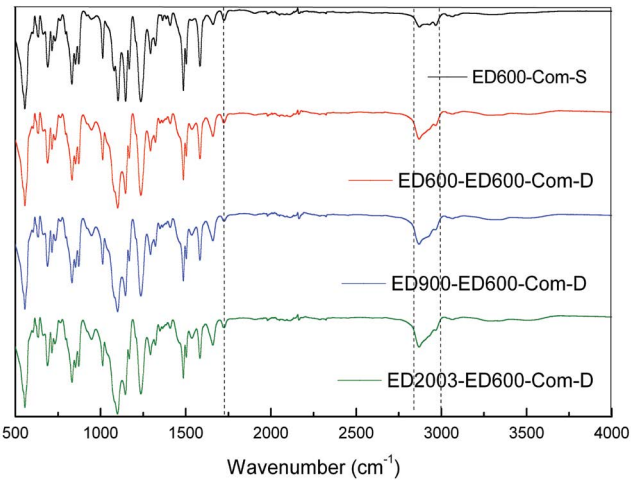

Fig. 3. FTIR spectra for composite membranes.

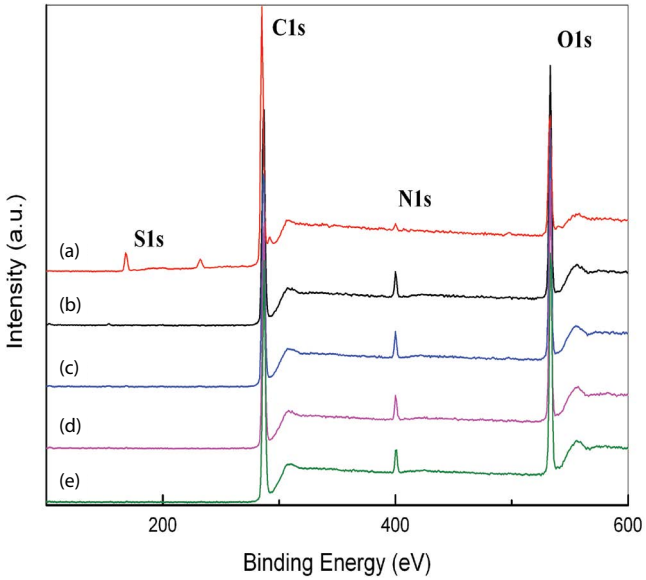

Fig. 4. XPS spectra for PSf substrate (a), ED600-Com-S (b), ED600-ED600-Com-D (c), ED900-ED600-Com-D (d), and ED2003-ED600-Com-D (e).

of oxygen and a lower proportion of carbon (Table 1). The increases in oxygen content and O/C ratio were the result of higher proportion of oxygen in jeffamine. With the increase in C–C–O repetitive units in jeffamine, the oxygen content increased; ED2003-ED600-Com-D contained the highest oxygen content, while ED900-ED600-Com-D contained the highest O/C ratio probably due to the different structure of C–C–O segment introduced in the second IP. ED600 with relative short chain might form the linear suspension structure in the second PEG-based layer as shown in Fig. 2. That is to say, one amino group in one jeffamine reacted with one chloroformyl group in second IP due to the relative short chain since the residual chloroformyl groups were not close enough to form two-end-linked structure. When ED2003 was used, the relative long chain probably made two amino groups in one jeffamine react with two chloroformyl groups. That is to say, ED2003 in membranes might form two-end-linked structure as shown in Fig. 2. The obvious decrease in nitrogen content for ED2003-ED600-Com-D might support this contention. When ED900 was used, some formed two-end-linked structures and some formed linear suspension structures. The peak for sulfur element was absent in the spectra of the composite membrane, indicating the complete coverage of the PSf substrate by the PA layer and the long PEG-based chain. The change in surface elemental compositions for membranes confirmed that jeffamine molecules were introduced into the composite membranes. The first and second IP processes were successful.

Table 1
XPS results of membranes

Membranes	Atomic percent (%)			Atomic ratio	
	O	N	C	O/N	O/C
PSf substrate	16.92	1.30[a]	78.39	13.02	0.216
ED600-Com-S	24.70	3.96	70.78	6.23	0.350
ED600-ED600-Com-D	24.87	3.86	70.80	6.44	0.350
ED900-ED600-Com-D	25.47	3.95	70.16	6.42	0.363
ED2003-ED600-Com-D	25.53	3.51	70.96	7.27	0.359

[a]From the residual solvent.

The high-resolution C1s spectra are shown in Fig. 5. The area percentage of peak at about 285 eV assigned to C–C bond decreased from 63.65% for PSf substrate to 26.28% for ED600-Com-S due to abundant C–C–O units in jeffamine and also decreased with the increase in C–C–O repetitive units in jeffamine used in the second IP. Compared with PSf substrate, the peaks at about 288 eV assigned to C=O bonds occur in composite membranes, indicating the successful reaction between chloroformyl group and amino group on PSf substrate. The peaks at about 287 eV assigned to C–O and C–N bonds occurred in composite membranes, indicating the successful introduction of C–C–O chain. Compared with ED600-Com-S, the area percentage of C–O/C–N bonds and the area ratio of C–O/C–N over C=O for membranes with the second IP increased, which further increased as the C–C–O repetitive units increased in jeffamine used in the second IP, indicating the successful proceeding of the second IP.

3.2. Morphology

The surface and cross-sectional morphologies of membranes are shown in Figs. 6 and 7. All the composite membranes were asymmetric structures, containing finger-like voids and dense skins. The cross-sectional morphology has no distinguished difference between membranes with single-layered PEG-based structure and membranes with double-layered PEG-based structure. As shown in Fig. 7, porous structure with a diameter of about 0.35 μm was observed in PSf substrate, while after IP, surface pores were covered by the selective layers and dense skins were observed in composite membranes. It could also be found that the composite membrane had the rougher skin compared with the PSf substrate. The grainy surface was the typical structure of PA on flat sheet NF membranes formed by IP when using aliphatic amines [21,22]. And after the second IP, nodules became larger, which was caused by the formation of new regular nodules due to the connection or aggregation of grafted PEG chains in dry state [23]. Moreover, this phenomenon was more distinct for long-chain ED2003 than that of short-chain ED600.

AFM images are also presented in Fig. 8 in order to more intuitively observe the stereo structure and obtain the roughness of membrane surface. The results showed an increase in the roughness of membrane surface after the first IP due to the formation of the grainy structure. Compared with the membranes with single-layered PEG-based structure, the membranes with double-layered PEG-based structure had smoother surface with a noticeably reduced surface roughness after the second IP for grafting the PEG-based brush layer in most cases, which were consistent with the results in some other reports [24]. The smooth surface is generally considered favorable to the alleviation of the adsorptions of foulants on membrane surface [25].

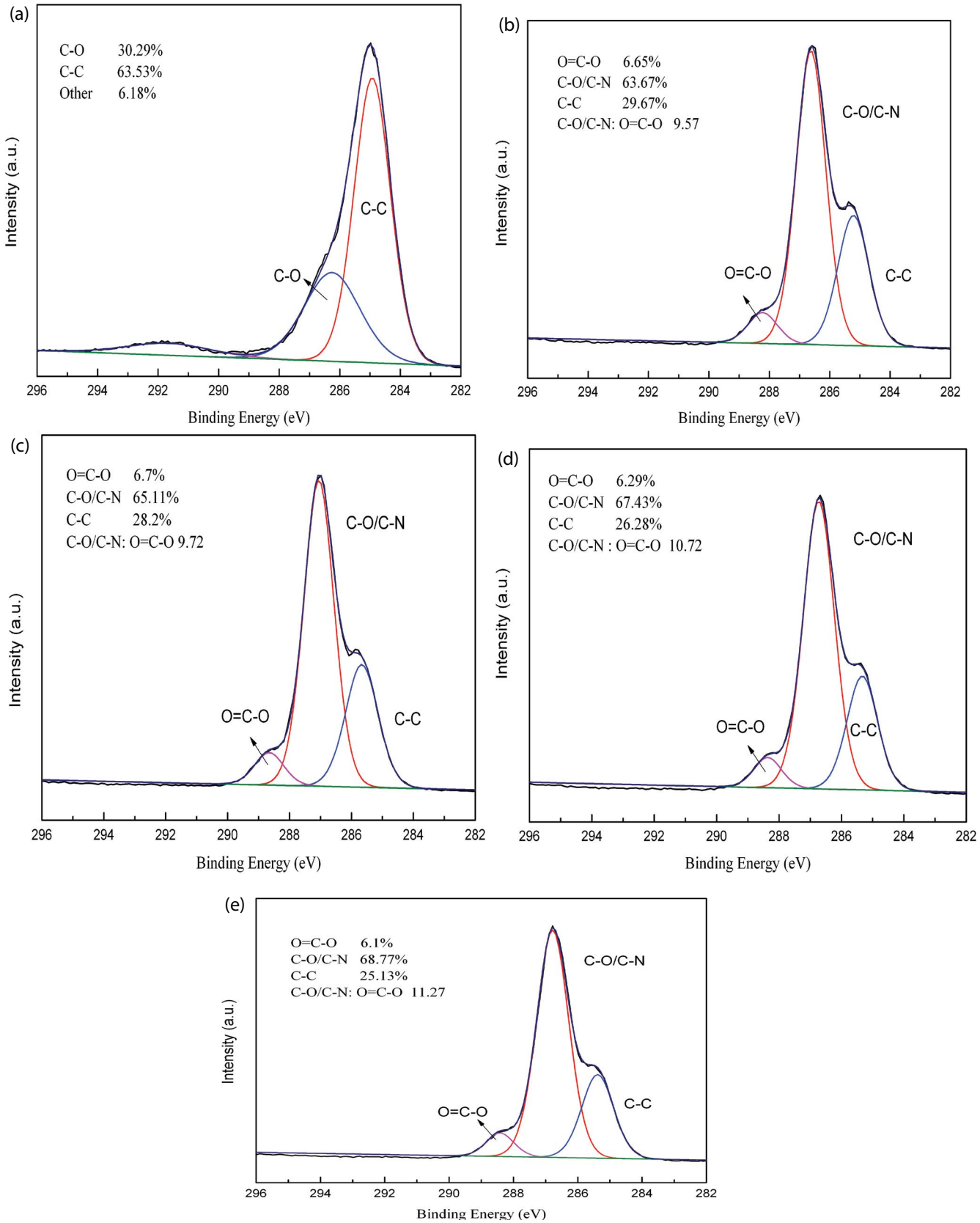

Fig. 5. High-resolution C1s spectra of detection for PSf substrate (a), ED600-Com-S (b), ED600-ED600-Com-D (c), ED900-ED600-Com-D (d), and ED2003-ED600-Com-D (e).

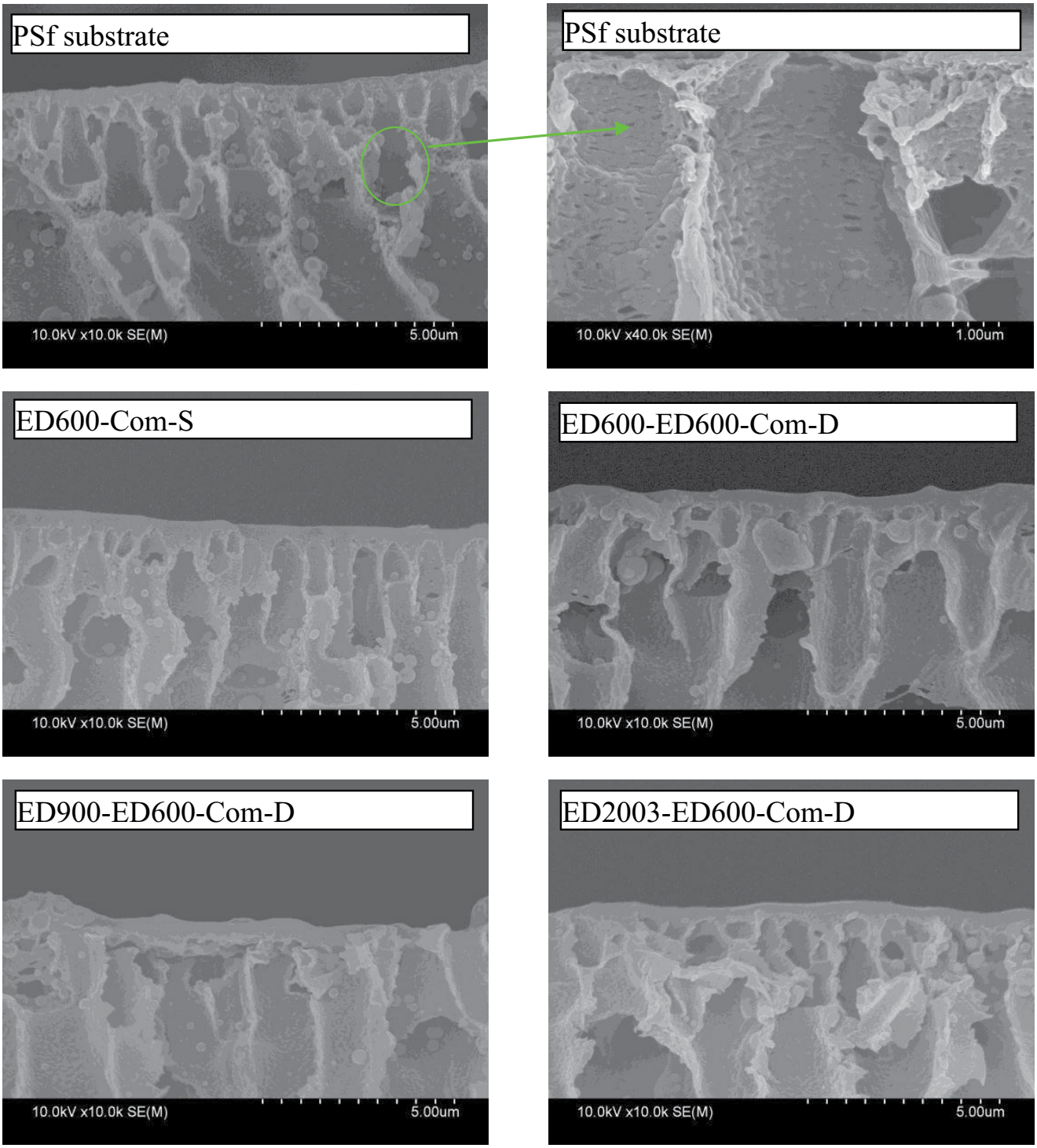

Fig. 6. Cross-sectional FESEM images of PSf substrate and composite membranes.

3.3. Surface hydrophilicity and charge characteristics

Surface hydrophilicity of membranes was characterized by contact angle as shown in Fig. 9. All the composite membranes had lower contact angles compared with PSf substrate due to the introduction of C–C–O segment from jeffamine. All the composite membranes with double-layered PEG-based structure had lower contact angles compared with the corresponding composite membranes with single-layered PEG-based structure due to higher coverage of C–C–O segment. ED2003-ED600-Com-D had lower contact angles compared with ED900-ED600-Com-D and ED600-ED600-Com-D, which was also due to higher coverage of C–C–O segment confirmed by the XPS results in Fig. 5 and Table 1.

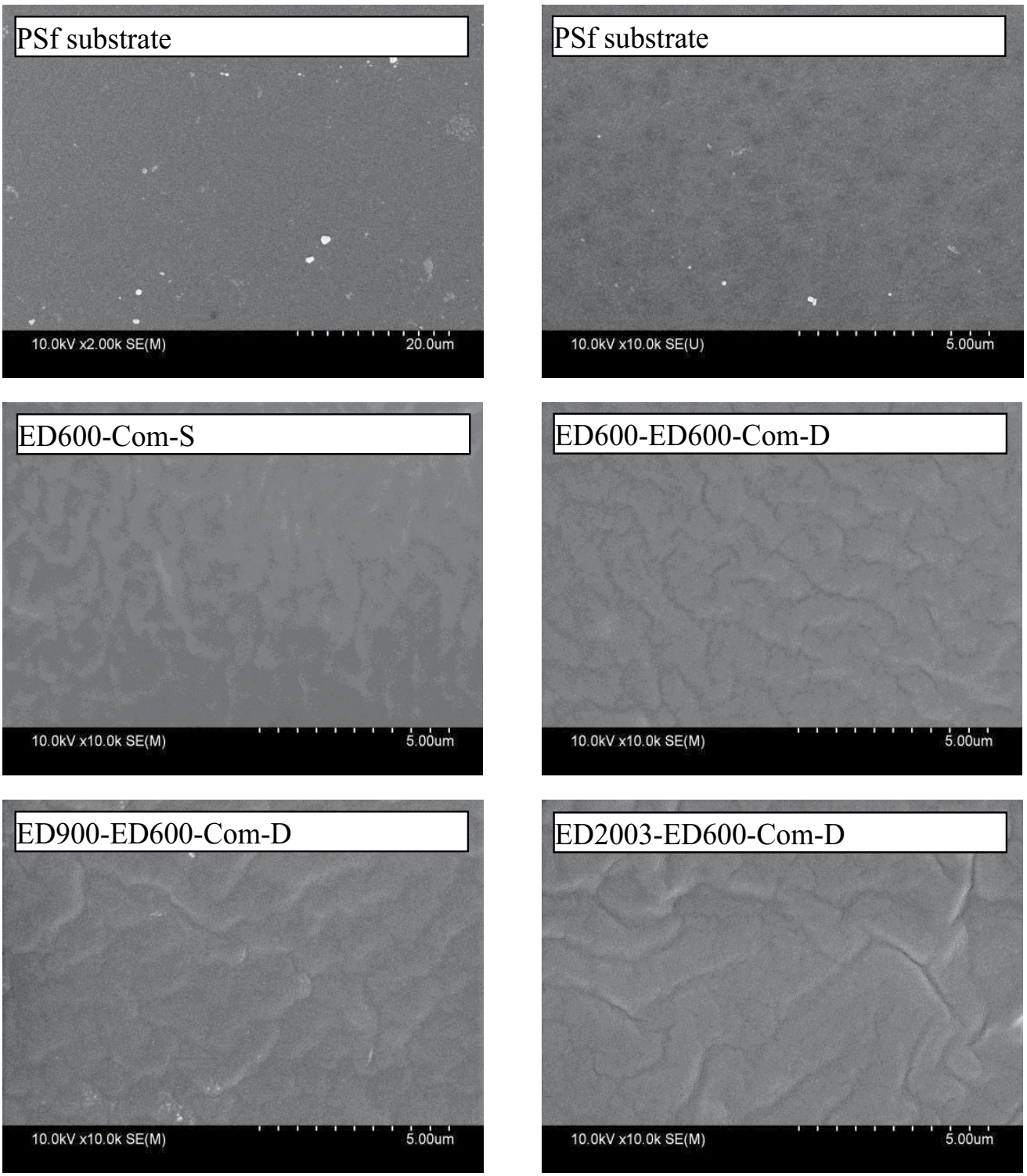

Fig. 7. Surface FESEM images of PSf substrate and composite membranes.

Surface change character of membranes was characterized by surface zeta-potential as shown in Fig. 10. Compared with PSf substrate, ED600-Com-S had higher negative zeta-potential due to the deprotonation of –COOH groups from the partial hydrolysis of the chloroformyl group of TMC that occurred after the first IP [26].

3.4. Permeation-separation properties of composite membranes

The permeation-separation properties of composite membranes were evaluated by using pure water flux and $MgSO_4$ rejection, and the results are shown in Figs. 11 and 12. Using aliphatic amine (jeffamine) in the first IP resulted in

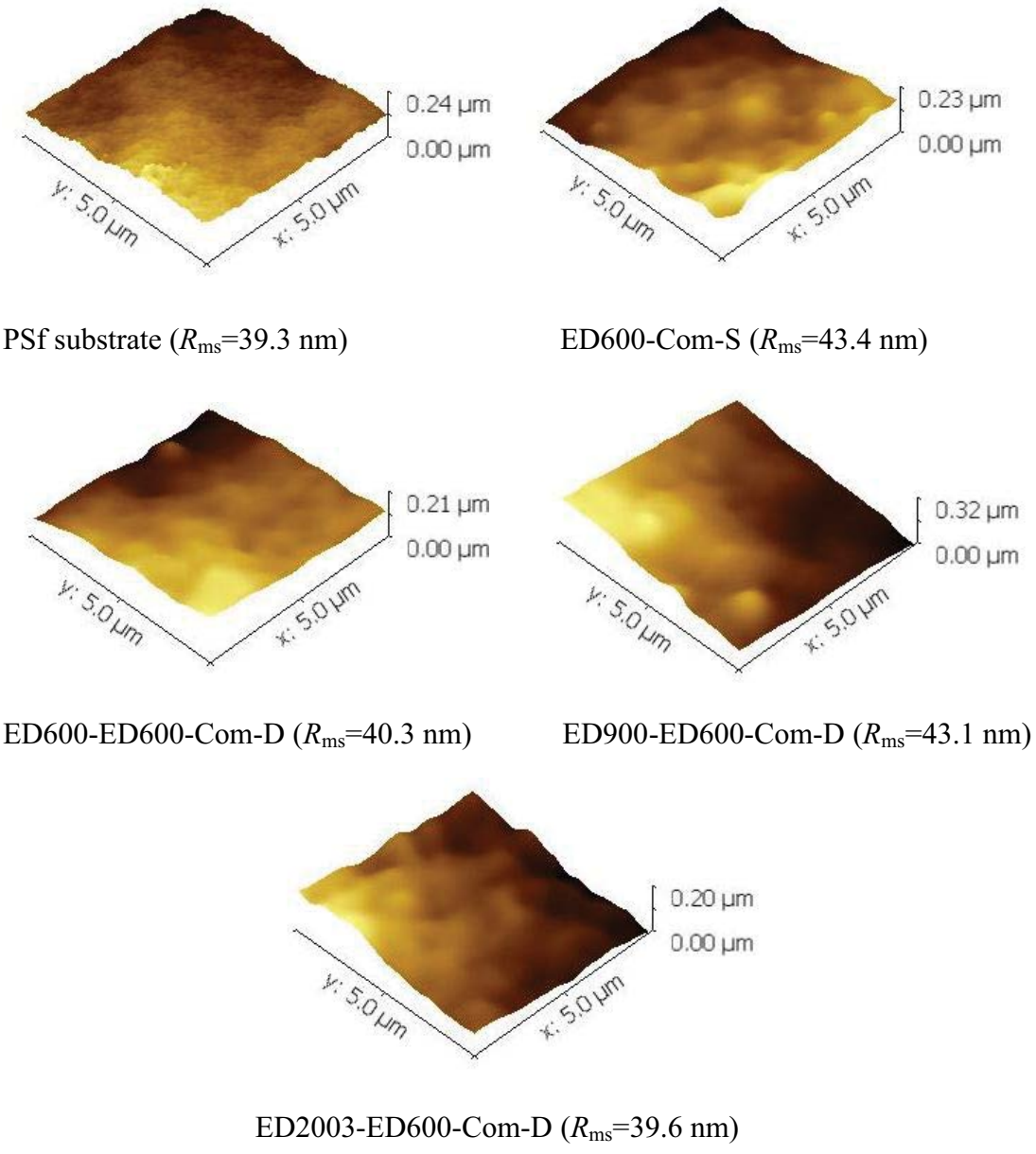

Fig. 8. AFM images of PSf substrate and composite membranes.

the low $MgSO_4$ rejection. Combination with other small molecule aqueous monomer (e.g. tris(2-aminoethyl)amine, metaphenylene diamine, and PIP) in the first IP can increase the rejection of $MgSO_4$, as illustrated in supplemental information. We also tested the dye rejection to determine the MWCO of composite membranes; the rejections of Rhodamine B for all the composite membranes were about 18%, the rejections for Bromophenol blue are about 30%, and those for Congo red were about 93%, indicating that the MWCO should be about 697 Da.

In this study, an interesting result was found that both of the pure water flux and rejection of composite membranes with double-layered PEG-based structure increased slightly compared with those of composite membranes with single-layered PEG-based structure, except ED900-ED600-Com-D. Even for ED900-ED600-Com-D, the decreases in pure water flux (2.8%) and rejection (0.25%) were tiny. It indicated that the second PEG-based layer made little contribution to the mass transfer resistance. The slight increase in pure water flux was mainly contributed by the increase in hydrophilicity. Although the zeta-potential increased, meaning the decrease in surface change, the composite membranes with double-layered PEG-based structure had slight higher rejections than composite membranes with single-layered PEG-based structure as a result of the slight increase in water flux. Entirely different results had previously been reported about RO/FO membranes modified with PEG-based layer, where the water flux was shown to decrease by up to 35%–50% upon surface PEG grafting [19,23,27]. The increase in rejection confirmed that the second IP did not destroy the compactness and

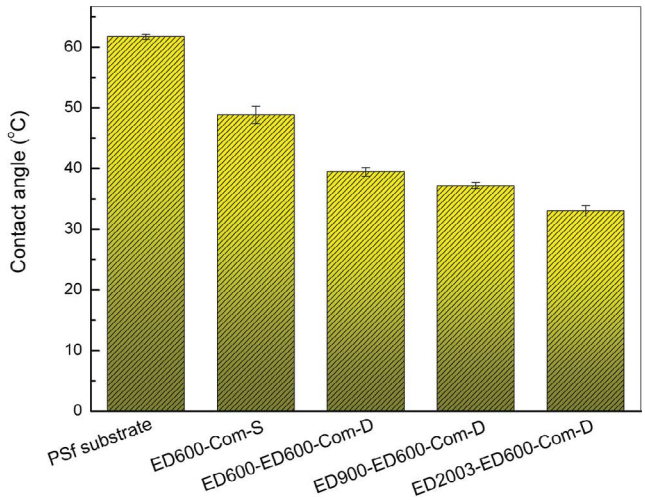

Fig. 9. Contact angles of PSf substrate and composite membranes.

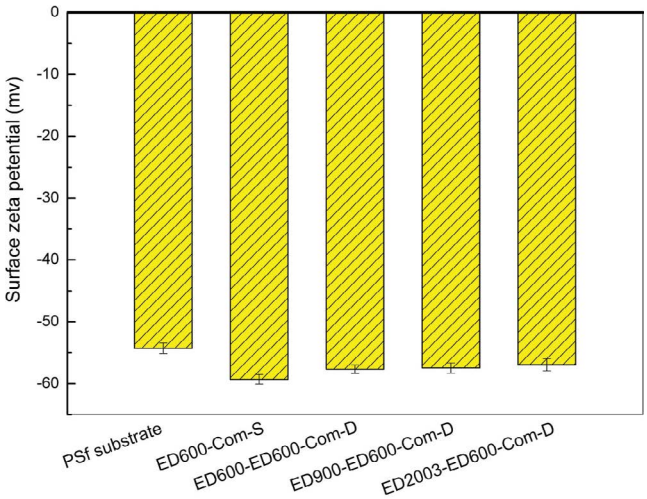

Fig. 10. Surface zeta-potentials of PSf substrate and composite membranes.

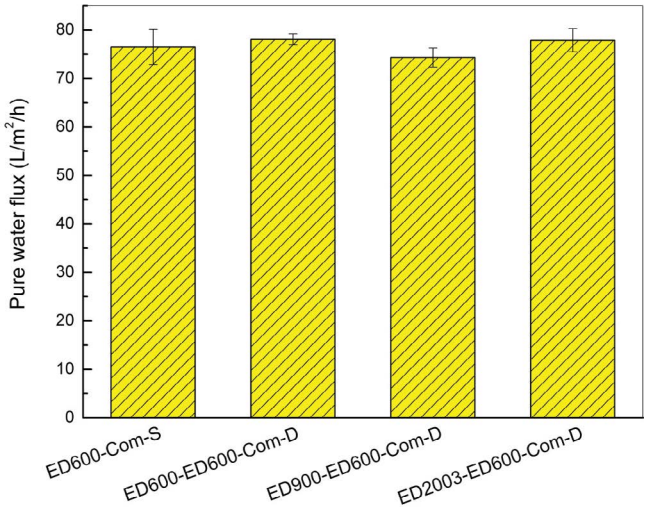

Fig. 11. Pure water fluxes of composite membranes.

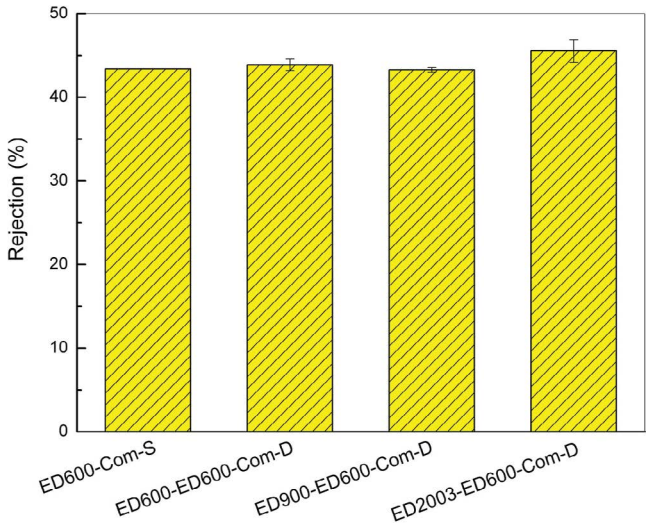

Fig. 12. $MgSO_4$ rejections of composite membranes.

integrity of the selective layer, which also indicated that this totally different result about the water flux might be obtained from the different graft density. As seen in Table 1, the oxygen content and O/C ratio increased slightly (0.69%, 3.1%, and 4.2% for oxygen content; 0%, 3.7%, and 2.6% for O/C ratio) after the second IP in this study, indicating low graft density. In other cases, the oxygen content and O/C ratio increased evidently after grafting (8.5% for O/C ratio [19], 29.1% for O/C ratio, and 24.7% for oxygen content [23]), indicating higher graft density, which led to an increase in mass transfer resistance and then a decrease in water flux. The performances of some similar state-of-the-art membranes are shown in Table 2 for comparison. Obviously, the composite membrane in this study showed an excellent property.

3.5. Antifouling properties of composite membranes

The process for measuring the antifouling performance of the composite membranes with single-layered or double-layered PEG-based structure and the change of water flux are shown in Fig. 13. The DRt and water FRR of the fabricated composite membranes are summarized in Figs. 14 and 15. When using the pure water as the feed solution in the first procedure during the first 60 min, the water flux declines slightly for all composite membranes with double PEG-based layers. In some cases, the water fluxes increased slightly. The worst flux recession occurred in ED600-Com-S with a decrease by about 10%. However, the water flux decreased significantly when the pure water was replaced by the BSA solution. As shown in Figs. 14 and 15, composite membranes with double-layered PEG-based structure had lower DRt and higher FRR than that with single-layered PEG-based structure, indicating that the double-layered PEG-based structure enhanced the antifouling properties.

We also found that composite membranes used ED600 and ED900 in the second IP had better antifouling performances compared with composite membranes that used ED2003. As we mentioned before, ED2003 formed the two-end-linked structure in the second IP as shown in Fig. 2,

Table 2
Comparison of separation performances for nanofiltration membranes

Modifier	Membrane structure	Water flux (L m^{-2} h^{-1})	Operate pressure (MPa)	Rejection	Ref.
Zwitterionic polyelectrolyte	Composite	91.6	1.6	97% (NaCl)	[28]
Carboxyl groups	Composite	49	0.6	44% ($MgSO_4$)	[29]
Graphene oxide	Composite	38.4	0.8	80% ($MgSO_4$)	[30]
$Ce(NO_3)_3$ nanoparticles	Composite	60.8	0.4	96.9% (methyl blue)	[31]
Triethylenetetramine functionalized multiwall carbon nanotube	L-S asymmetric	97.7	1.0	46% ($MgSO_4$)	[32]
Zeolitic imidazolate framework-8	Composite	55.0	0.6	95% (Na_2SO_4)	[33]
PEG segment	Composite	78.1	0.5	46% ($MgSO_4$)	This study
		41.8	0.5	85% ($MgSO_4$)	This study[a]

[a]In supplemental information.

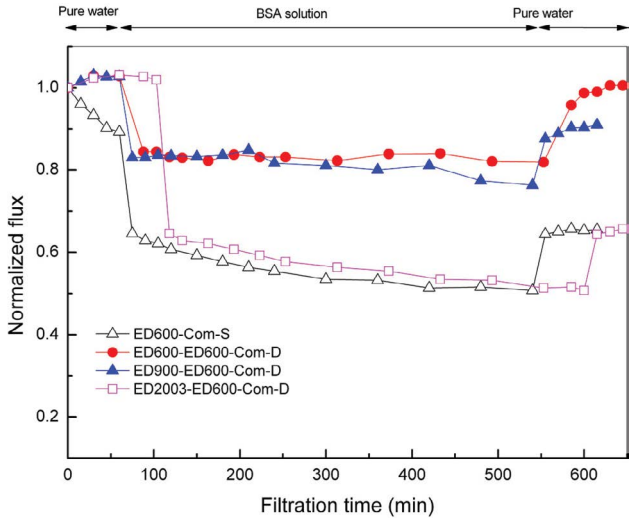

Fig. 13. The process of the fouling experiments and the time dependence of water fluxes of fabricated composite membranes.

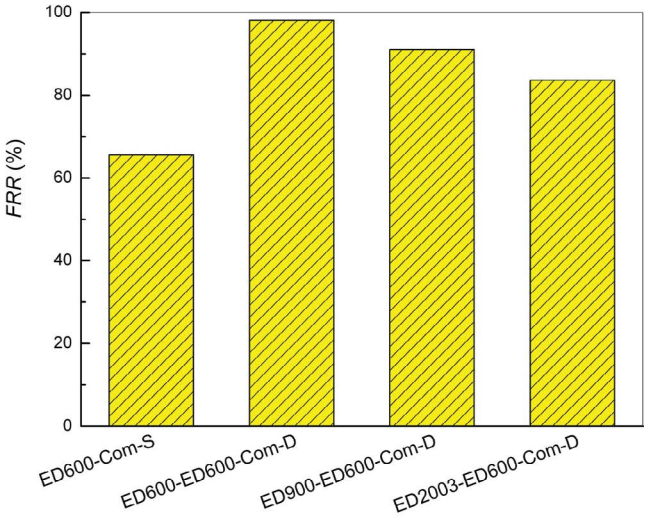

Fig. 15. Water flux recovery ratio for fabricated composite membranes.

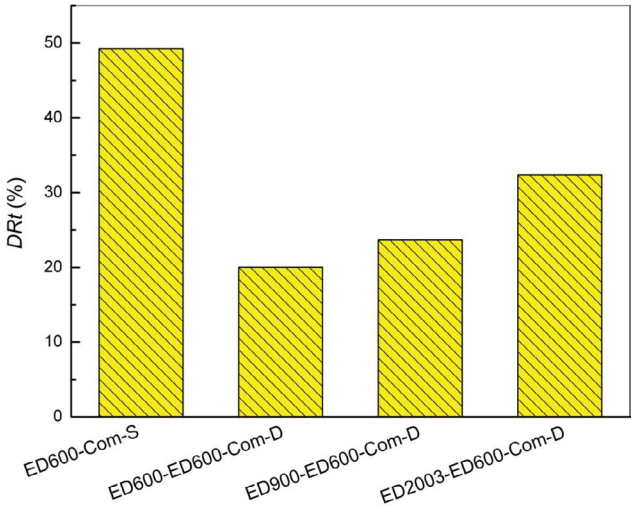

Fig. 14. Total flux decline ratio of water for fabricated composite membranes.

while ED600 formed the linear suspension structure. For ED900, some might form two-end-linked structure and some might form linear suspension structure. It indicated that the linear suspension PEG-based layer improved the antifouling properties more than the two-end-linked layer. The ratio of reversible fouling over total fouling and the ratio of irreversible fouling over total fouling for composite membranes are shown in Fig. 16. It was obvious that the composite membranes with double-layered PEG-based structure had the higher ratio of reversible fouling than the corresponding composite membranes with single-layered PEG-based structure, except ED2003-ED600-Com-D. And the ratio of reversible fouling decreased as the increase in chain length used in the second IP. As mentioned before, the second PEG-based layer in ED2003-ED600-Com-D was also two-end-linked structure, but not linear suspension structure, which might be the reason for the lowest ratio of reversible fouling. It indicated that the linear suspension structure was responsible for the reversible fouling. On the whole, membranes using ED600 in the second IP had the best antifouling performance, no

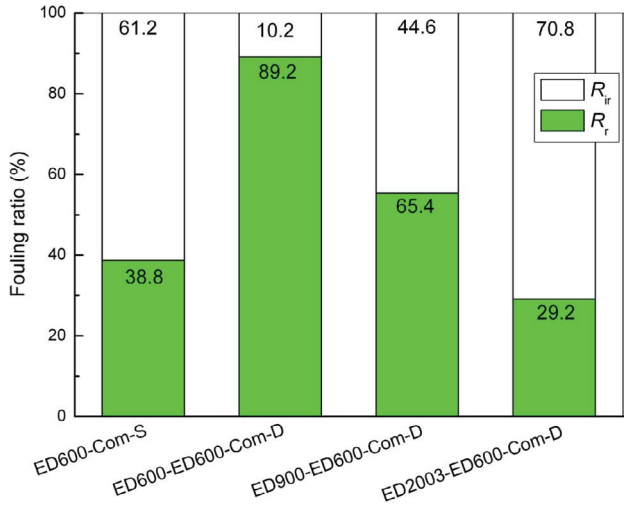

Fig. 16. The ratio of reversible fouling over total fouling and the ratio of irreversible fouling over total fouling for composite membranes.

matter from DRt, FRR, and the ratio of reversible fouling, and then the membranes using ED900. Therefore, it could be concluded that the linear suspension PEG-based structure improved the antifouling properties significantly.

4. Conclusion

In this study, composite membranes with single-layered or double-layered PEG-based structure were fabricated by one-step or two-step IP with jeffamine as the antifouling modifier. The hydrophilic C–C–O segment was in the main chain in the selective layer synthesized by the first IP. By using different monomers with different chain lengths in the second IP, C–C–O segment formed linear suspension structure or two-end-linked structure in the additional PEG-based layer. The additional layer improved the surface hydrophilicity and reduced the surface roughness. The second IP did not destroy the selective layer with almost no decrease in the rejection of $MgSO_4$. The additional layer did not increase the mass transfer resistance with almost no loss of the pure water flux. And in some cases, the pure water flux and rejection even increased slightly. The PEG-based structure improved the antifouling performance, especially the additional layer which decreased the BSA fouling and led to lower water flux decline ratio and higher water FRR compared with the corresponding composite membranes with single PEG-based layer. And the linear suspension PEG-based structure was more efficient to improve the antifouling properties than the two-end-linked structure. The additional PEG-based layer with linear suspension structure increased the reversible fouling ratio, which finally led to the highest water FRR of 99.6% after pure water cleaning.

Acknowledgments

This work was supported by the National Natural Science Foundation of China (Grant No. 21776217) and Technology Plans of Tianjin (No. 17PTSYJC00050 and 18PTSYJC 00190).

References

[1] M. Paul, S.D. Jons, Chemistry and fabrication of polymeric nanofiltration membranes: a review, Polymer, 103 (2016) 417–456.
[2] A. Akbaria, R. Yegania, B. Pourabbasb, A. Behboudia, Analysis of antifouling behavior of high dispersible hydrophilic poly(ethylene glycol)/vinyl functionalized SiO_2 nanoparticles embedded polyethylene membrane, Desal. Wat. Treat., 76 (2017) 83–97.
[3] H. Wang, J. Ren, A. Hlaing, M.D. Yan, Fabrication and anti-fouling properties of photochemically and thermally immobilized poly(ethylene oxide) and low molecular weight poly(ethylene glycol) thin films, J. Colloid Interface Sci., 354 (2011) 160–167.
[4] V. Ghaffarian, S.M. Mousavi, M. Bahreini, H. Chamani, Poly(butylene succinate)/polyethersulfone/poly(ethylene glycol) membrane: influence of additive molecular weight and concentration on morphology, properties, and performance of the membrane, Desal. Wat. Treat., 57 (2016) 22191–22199.
[5] S. Zhang, G.L. Qiu, Y.P. Ting, T.-S. Chung, Silver-PEGylated dendrimer nanocomposite coating for anti-fouling thin film composite membranes for water treatment, Colloids Surf., A, 436 (2013) 207–214.
[6] L. Shen, C. Cheng, X. Yu, Y. Yang, X. Wang, M. Zhu, B.S. Hsiao, Low pressure UV-cured CS-PEO-PTEGDMA/PAN thin film nanofibrous composite nanofiltration membranes for anionic dye separation, J. Mater. Chem. A, 4 (2016) 15575–15588.
[7] C. Wang, G.K. Such, A. Widjaya, H. Lomas, G. Stevens, F. Caruso, S.E. Kentish, Click poly(ethylene glycol) multilayers on RO membranes: fouling reduction and membrane characterization, J. Membr. Sci., 409–410 (2012) 9–15.
[8] F.-X. Perrin, T.D.H. Nguyen, D.L. Nguyen, Formation, structure and antibacterial activities of silazane networks grafted with poly(ethylene glycol) branches, Prog. Org. Coat., 88 (2015) 92–105.
[9] T.H.A. Ngo, S. Mori, D.T. Tran, Photo-induced grafting of poly(ethylene glycol) onto polyamide thin film composite membranes, J. Appl. Polym. Sci., 134 (2017) 45454.
[10] A. Akthakul, R.F. Salinaro, A.M. Mayes, Antifouling polymer membranes with subnanometer size selectivity, Macromolecules, 37 (2004) 7663–7668.
[11] R.M. Gol, A. Bera, S. Banjo, B. Ganguly, S.K. Jewrajka, Effect of amine spacer of PEG on the properties, performance and antifouling behavior of poly(piperazineamide) thin film composite nanofiltration membranes prepared by in situ PEGylation approach, J. Membr. Sci., 472 (2014) 154–166.
[12] R.M. Gol, S.K. Jewrajka, Facile in situ PEGylation of polyamide thin film composite membranes for improving fouling resistance, J. Membr. Sci., 455 (2014) 271–282.
[13] A. Bera, R.M. Gol, S. Chatterjee, S.K. Jewrajka, PEGylation and incorporation of triazine ring into thin film composite reverse osmosis membranes for enhancement of anti-organic and anti-biofouling properties, Desalination, 360 (2015) 108–117.
[14] D.S. Zhao, S.L. Yu, G.C. Liu, Q.B. Yuan, H.C. Guo, Polypiperazine-amide nanofiltration membrane incorporated with poly (ethylene glycol) derivative for electrodialysis concentrate treatment, Sep. Purif. Technol., 153 (2015) 43.
[15] X.Q. Cheng, L. Shao, C.H. Lau, High flux polyethylene glycol based nanofiltration membranes for water environmental remediation, J. Membr. Sci., 476 (2015) 95–104.
[16] X.Q. Cheng, Y.Y. Liu, Z.H. Guo, L. Shao, Nanofiltration membrane achieving dual resistance to fouling and chlorine for "green" separation of antibiotics, J. Membr. Sci., 493 (2015) 156–166.
[17] A. Asatekin, A. Menniti, S. Kang, M. Elimelech, E. Morgenroth, A.M. Mayes, Antifouling nanofiltration membranes for membrane bioreactors from self-assembling graft copolymers, J. Membr. Sci., 285 (2006) 81–89.
[18] L.F. Liu, D.Z. Xu, H.L. Chen, C.J. Gao, Novel polyamide-urea-imide composite reverse osmosis membrane prepared via two-step interfacial polymerization, Chin. J. Chem. Eng., 63 (2012) 1913–1921.

[19] X. Lu, S. Romero-Vargas Castrillón, D.L. Shaffer, J. Ma, M. Elimelech, In situ surface chemical modification of thin-film composite forward osmosis membranes for enhanced organic fouling resistance, Environ. Sci. Technol., 47 (2013) 12219–12228.
[20] J.H. Hu, X.F. Zhen, Practical Infrared Spectroscopy, Science press, Beijing, 2011.
[21] F. Li, Y.L. Su, Y.N. Dong, X.T. Zhao, Z.Y. Jiang, R.N. Zhang, J.J. Zhao, Separation performance of thin-film composite nanofiltration membrane through interfacial polymerization using different amine monomers, Desalination, 333 (2014) 59–65.
[22] R.J. Petersen, Composite reverse osmosis and nanofiltration membranes, J. Membr. Sci., 83 (1993) 81–150.
[23] G.D. Kang, H.J. Yu, Z.N. Liu, Y.C. Cao, Surface modification of a commercial thin film composite polyamide reverse osmosis membrane by carbodiimide-induced grafting with poly(ethylene glycol) derivatives, Desalination, 275 (2011) 252–259.
[24] C. Liu, J. Lee, J. Ma, M. Elimelech, Antifouling thin-film composite membranes by controlled architecture of zwitterionic polymer brush layer, Environ. Sci. Technol., 51 (2017) 2161–2169.
[25] V. Kochkodan, N. Hilal, A comprehensive review on surface modified polymer membranes for biofouling mitigation, Desalination, 356 (2015) 187–207.
[26] H.F. Wang, Q.F. Zhang, S.B. Zhang, Positively charged nanofiltration membrane formed by interfacial polymerization of 3,3′,5,5′-biphenyl tetraacyl chloride and piperazine on a poly(acrylonitrile) (PAN) support, J. Membr. Sci., 378 (2011) 243–249.
[27] S. Romero-Vargas Castrillón, X. Lu, D.L. Shaffer, M. Elimelech, Amine enrichment and poly(ethylene glycol) (PEG) surface modification of thin-film composite forward osmosis membranes for organic fouling control, J. Membr. Sci., 450 (2014) 331–339.
[28] S. Davari, M. Omidkhah, M. Abdollahi, Improved antifouling ability of thin film composite polyamide membrane modified by a pH-sensitive imidazole-based zwitterionic polyelectrolyte, J. Membr. Sci., 564 (2018) 788–799.
[29] S. Yuan, J. Li, J. Zhu, A. Volodine, J. Li, G. Zhang, P. Van Puyvelde, B. Van der Bruggen, Hydrophilic nanofiltration membranes with reduced humic acid fouling fabricated from copolymers designed by introducing carboxyl groups in the pendant benzene ring, J. Membr. Sci., 563 (2018) 655–663.
[30] G.S. Lai, W.J. Lau, P.S. Goh, A.F. Ismail, Y.H. Tan, C.Y. Chong, R. Krause-Rehberg, S. Awad, Tailor-made thin film nanocomposite membrane incorporated with graphene oxide using novel interfacial polymerization technique for enhanced water separation, Chem. Eng. J., 344 (2018) 524–534.
[31] Z. Gu, S. Cui, S. Liu, Q. An, Z. Qin, H. Guo, Superhydrophilic nanofiltration membrane with antifouling property through in-situ mineralization of $Ce_2(CO_3)_3$ nanoparticles, J. Taiwan Inst. Chem. Eng., 88 (2018) 70–77.
[32] M. Peydayesh, T. Mohammadi, O. Bakhtiari, Effective treatment of dye wastewater via positively charged TETA-MWCNT/PES hybrid nanofiltration membranes, Sep. Purif. Technol., 194 (2018) 488–502.
[33] F. Xiao, B. Wang, X. Hu, S. Nair, Y. Chen, Thin film nanocomposite membrane containing zeolitic imidazolate framework-8 via interfacial polymerization for highly permeable nanofiltration, J. Taiwan Inst. Chem. Eng., 83 (2018) 159–167.

Supplementary information

The cross-linking between the aliphatic monomer (jeffamine) and trimesoyl chloride resulted in the low rejection; in this section, some other small molecule aqueous monomers (piperazine (PIP), m-phenylenediamide (MPD), and tris(2-aminoethyl)amine (TAEA) were mixed with jeffamine to improve the rejection with the ratio of 3:7 (W/W). The characterization and performance are presented in Figs. S1–S11.

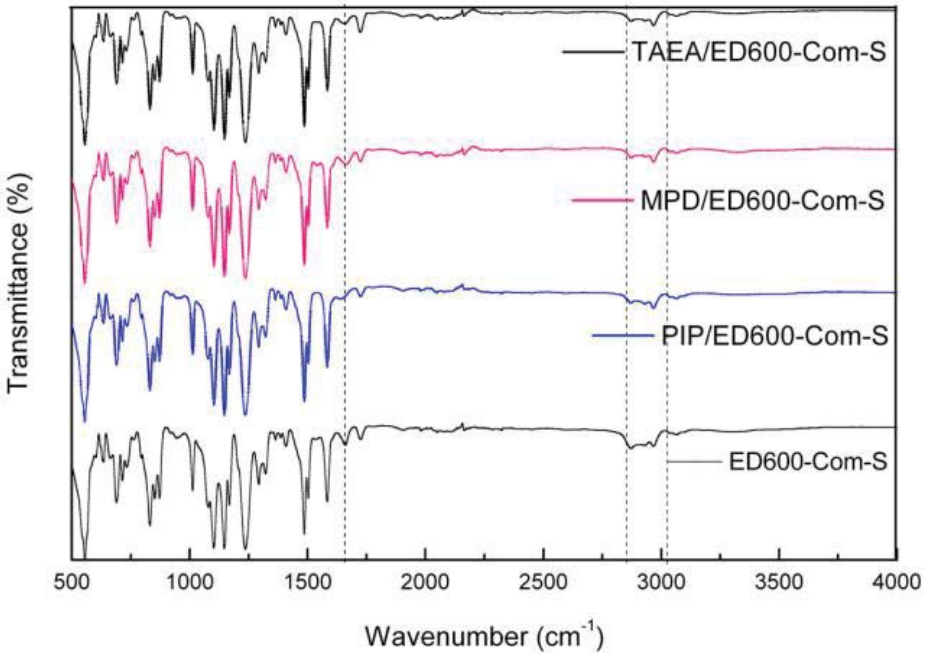

Fig. S1. FTIR spectra for composite membranes. After PIP and TAEA were incorporated into the polyamide matrix, the peak of amide shifted from 1,660 cm^{-1} to the lower wavenumber at 1,638 cm^{-1} for ED600/PIP-Com-S and 1,656 cm^{-1} for ED600/TAEA-Com-S. And after MPD was incorporated into the polyamide matrix, the peak of amide shifted from 1,660 cm^{-1} to the higher wavenumber at 1,663 cm^{-1} for ED600/MPD-Com-S due to the conjugation effect. All spectra showed broad characteristic peaks in the range of 2,880–3,000 cm^{-1} (–CH_2–), because of C–C–O repeat units in jeffamine.

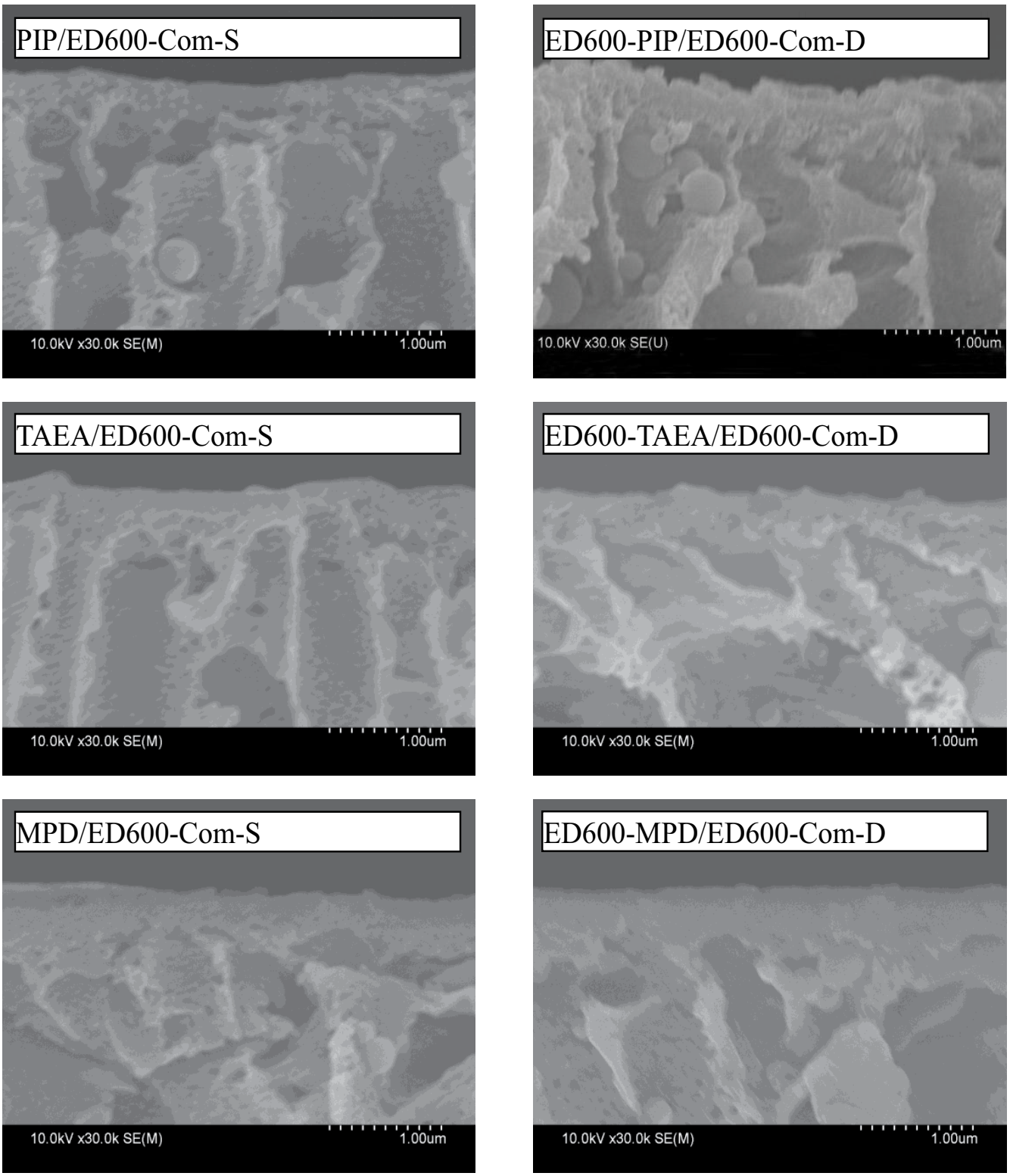

Fig. S2. Cross-sectional FESEM images of composite membranes.

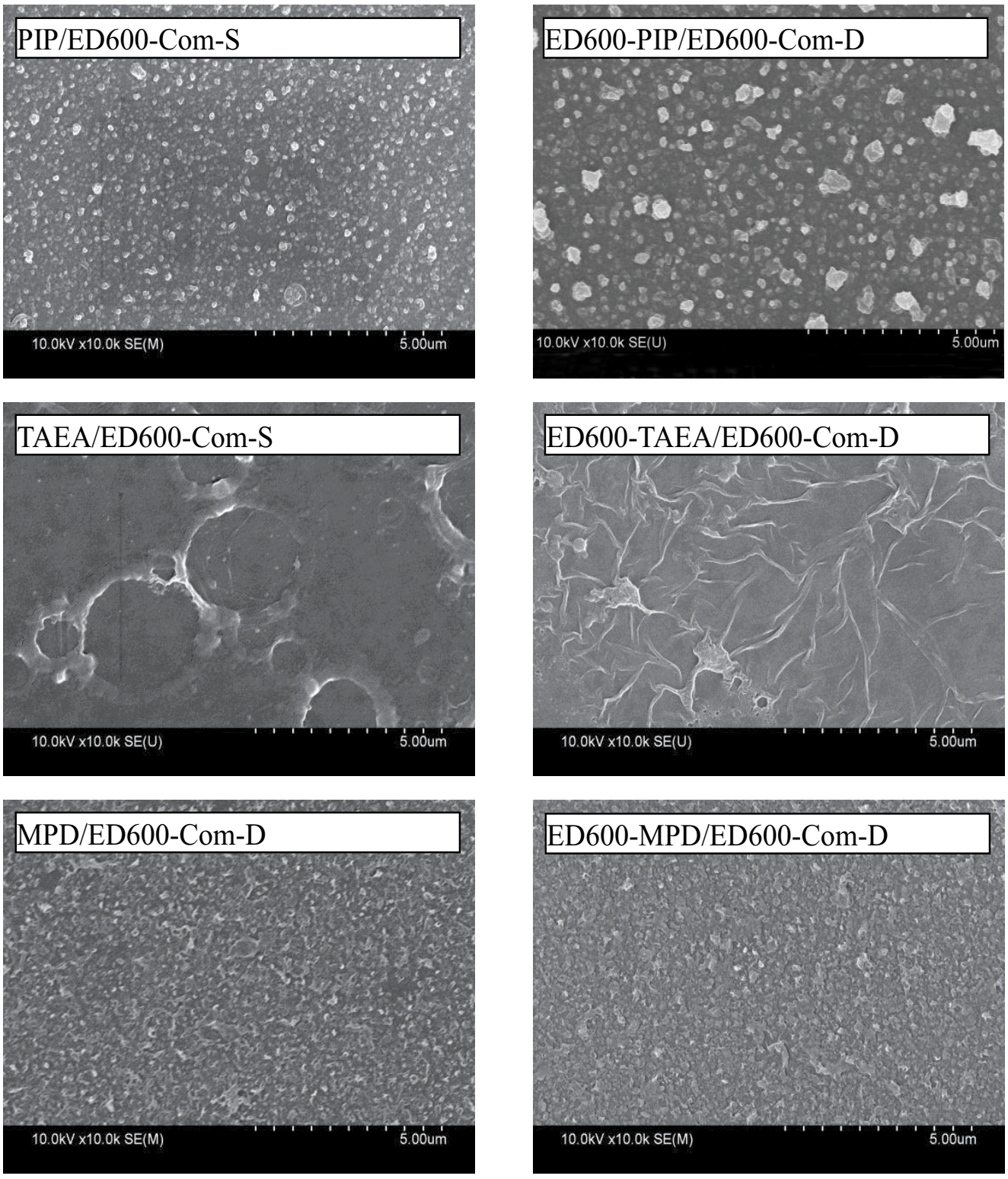

Fig. S3. Surface FESEM images of composite membranes. When incorporating MPD, a unique and characteristic ridge-and-valley structure was observed, which was the typical structure of PA surface when using aromatic amines. When incorporating PIP, nodular structure with a few dish-like bulges was observed, which was the typical characteristic of PA surface obtained from the polycondensation of TMC and PIP. When incorporating TAEA, "multi-layered" PA structure was observed, which contained a raised circular structure on PSf substrate and a widespread PA layer.

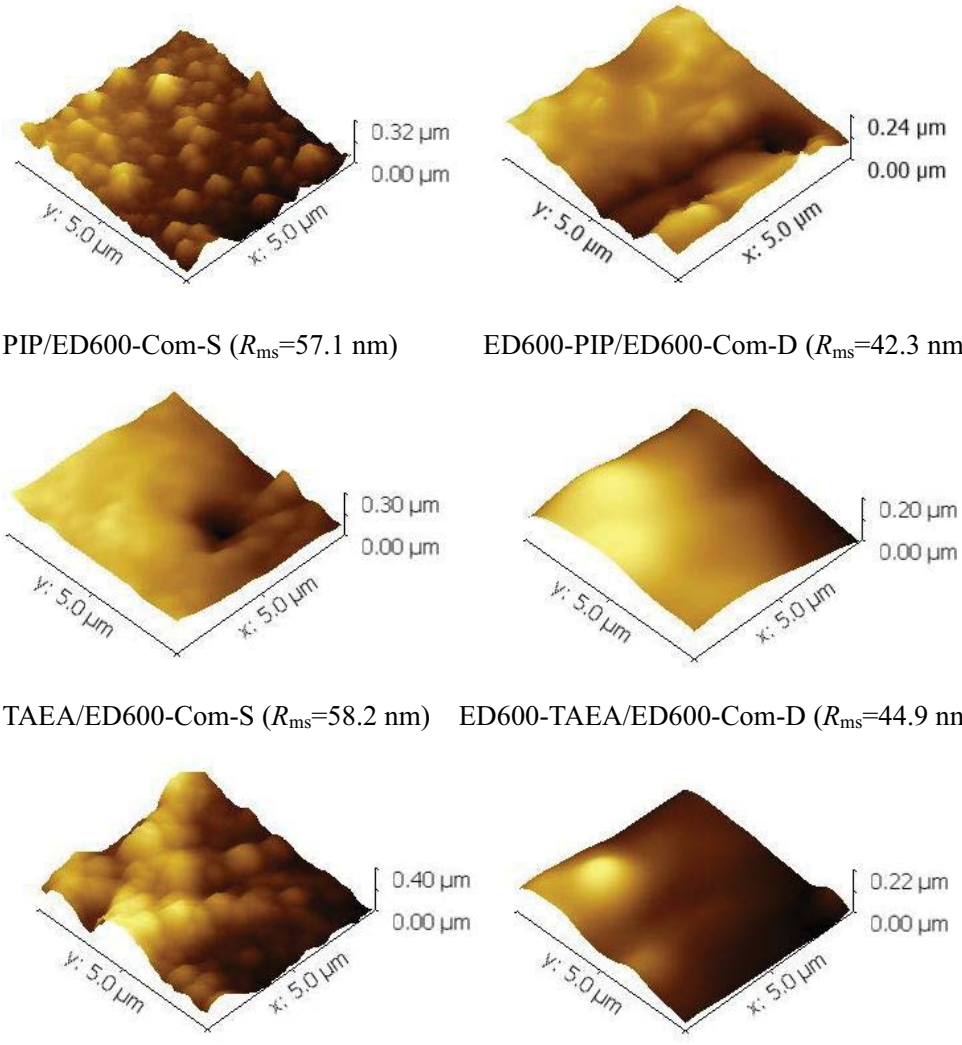

PIP/ED600-Com-S (R_{ms}=57.1 nm) ED600-PIP/ED600-Com-D (R_{ms}=42.3 nm)

TAEA/ED600-Com-S (R_{ms}=58.2 nm) ED600-TAEA/ED600-Com-D (R_{ms}=44.9 nm)

MPD/ED600-Com-S (R_{ms}=91.9 nm) ED600-MPD/ED600-Com-D (R_{ms}=45.4 nm)

Fig. S4. AFM images of composite membranes.

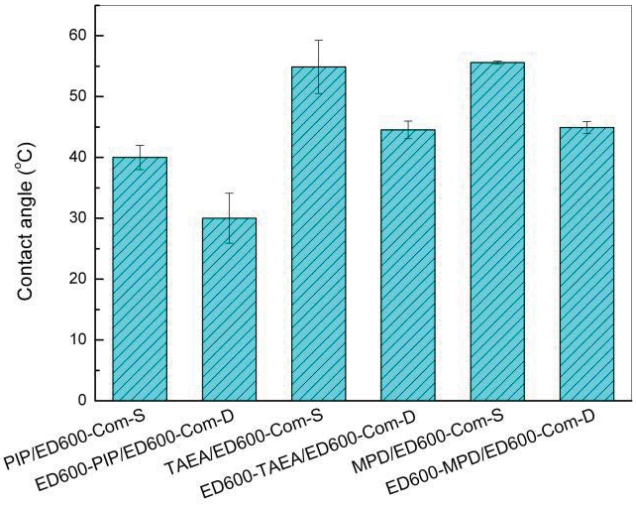

Fig. S5. Contact angles of composite membranes.

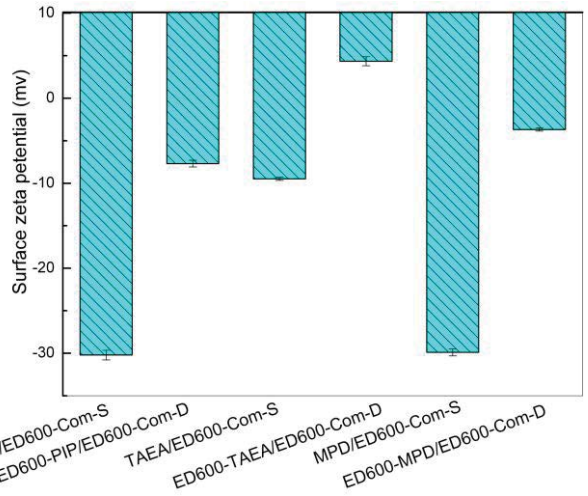

Fig. S6. Surface zeta-potentials of composite membranes.

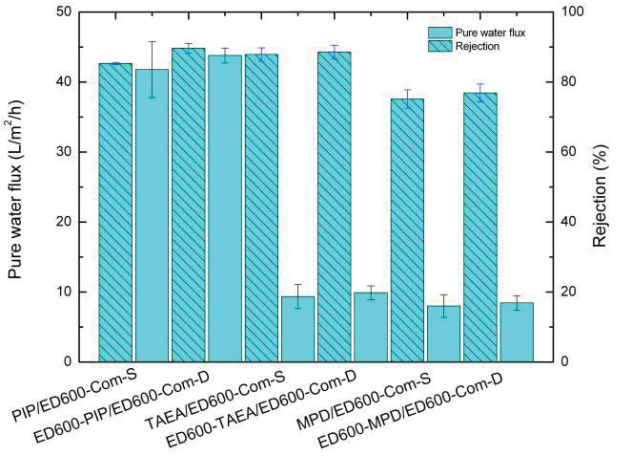

Fig. S7. Pure water fluxes and $MgSO_4$ rejections of composite membranes.

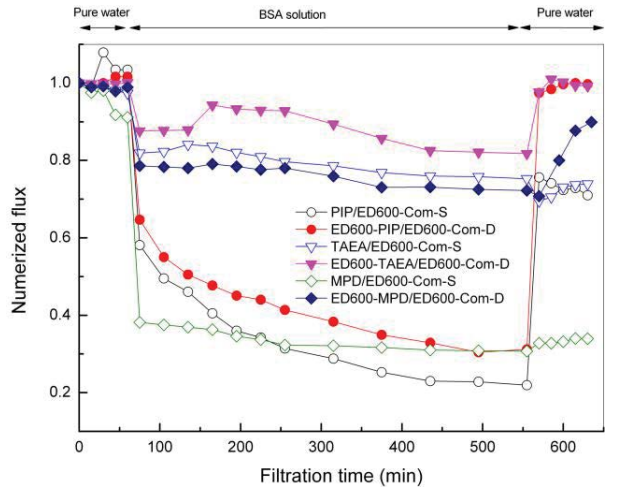

Fig. S8. The process of the fouling experiments and the time dependence of water fluxes of composite membranes.

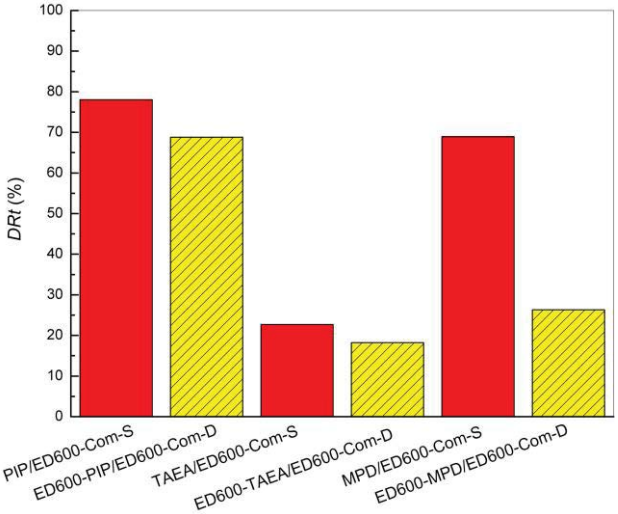

Fig. S9. Total flux decline ratio of water for composite membranes.

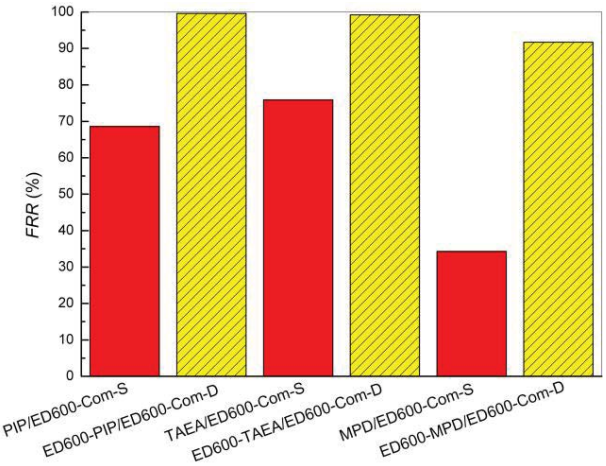

Fig. S10. Water flux recovery ratio for composite membranes.

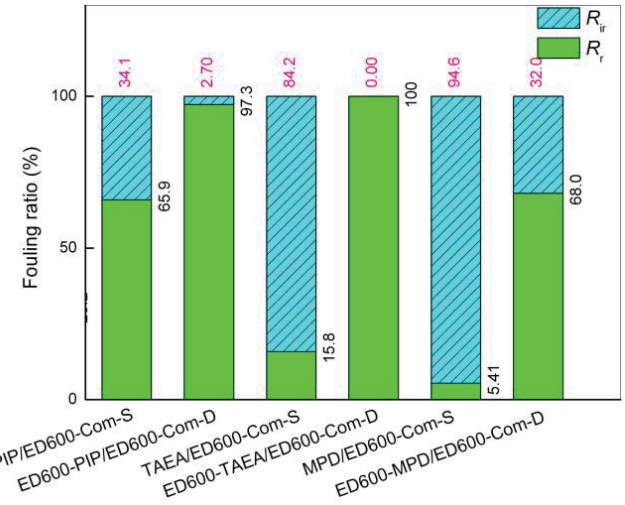

Fig. S11. The ratio of reversible fouling over total fouling and the ratio of irreversible fouling over total fouling for composite membranes.